



1 **The effect of viscosity on the HO₂ uptake by sucrose and**
2 **secondary organic aerosol particles**

3

4 Pascale S. J. Lakey^{1,2}, Thomas Berkemeier², Manuel Krapf³, Josef Dommen³, Sarah S. Steimer³,
5 Lisa K. Whalley^{1,4}, Trevor Ingham^{1,4}, Maria T. Baeza-Romero⁵, Ulrich Pöschl², Manabu Shiraiwa²,
6 Markus Ammann³, Dwayne E. Heard^{1,4,*}

7 ¹ *School of Chemistry, University of Leeds, Woodhouse Lane, Leeds, LS2 9JT, UK*

8 ² *Multiphase Chemistry Department, Max-Planck-Institute for Chemistry, Hahn-Meiter-Weg 1, 55128*
9 *Mainz, Germany.*

10 ³ *Paul Scherrer Institute, Villigen, Switzerland.*

11 ⁴ *National Centre for Atmospheric Chemistry, University of Leeds, Woodhouse Lane, Leeds, LS2 9JT,*
12 *UK*

13 ⁵ *Escuela de Ingeniería Industrial de Toledo, Universidad de Castilla la Mancha, Avenida Carlos III*
14 *s/n Real Fábrica de Armas, Toledo, 45071, Spain*

15

16 * *Corresponding author: Dwayne Heard (D.E.Heard@leeds.ac.uk)*

17

18

19 **Abstract**

20

21 We report the first measurements of HO₂ uptake coefficients, γ , for secondary organic aerosol particles
22 (SOA) and for the well-studied model compound sucrose which was doped with copper. Above 65%
23 relative humidity (RH), γ for copper doped sucrose aerosol particles equalled the surface mass
24 accommodation coefficient $\alpha = 0.22 \pm 0.06$ but decreased to $\gamma = 0.012 \pm 0.007$ upon decreasing the RH
25 to 17 %. The trend of γ with RH can be explained by an increase in aerosol viscosity, as demonstrated
26 using the kinetic multi-layer model of aerosol surface and bulk chemistry (KM-SUB). SOA from two
27 different precursors, α -pinene and 1,3,5-trimethylbenzene (TMB), was investigated, yielding small
28 uptake coefficients of $\gamma < 0.001$ and $\gamma = 0.004 \pm 0.002$, respectively. It is postulated that the larger values
29 measured for TMB derived SOA compared to α -pinene derived SOA are either due to differing
30 viscosity, a different liquid water content of the aerosol particles or a HO₂ + RO₂ reaction occurring
31 within the aerosol particles.

32



33 1. Introduction

34

35 OH and HO₂ radicals play a vital role in atmospheric chemistry by controlling the oxidative
36 capacity of the troposphere, with HO₂ acting as a short-lived reservoir for OH. Oxidation by the OH
37 radical determines the lifetime and concentrations of many trace gases within the troposphere such as
38 NO_x (NO and NO₂), CH₄ and volatile organic compounds (VOCs). The reaction of HO₂ with NO also
39 constitutes an important source of ozone, which is damaging to plants, a respiratory irritant and a
40 greenhouse gas (Pöschl and Shiraiwa, 2015;Fowler et al., 2009). It is therefore important to have a
41 thorough understanding of the reactions and processes that affect HO_x concentrations. However, during
42 field campaigns HO₂ concentrations have sometimes been measured as being lower than the
43 concentrations predicted by constrained box models implying a missing HO₂ sink, which has often been
44 attributed to HO₂ uptake by aerosol particles (e.g. (Kanaya et al., 2007;Mao et al., 2010;Whalley et al.,
45 2010)).

46 SOA is generated from low-volatility products formed by the oxidation of VOCs, and it
47 accounts for a large fraction of the organic matter in the troposphere. For example, in urban areas it can
48 account for up to 90 % of the organic particulate mass (Kanakidou et al., 2005;Lim and Turpin, 2002).
49 Lakey et al. (2015a) previously measured the HO₂ uptake coefficient onto single component organic
50 aerosol particles as ranging from $\gamma < 0.004$ to $\gamma = 0.008 \pm 0.004$ unless elevated transition metal ions,
51 that catalyse the destruction of HO₂, were present within the aerosol. Taketani et al. (2013) and Taketani
52 and Kanaya (2010) also measured the HO₂ uptake coefficient onto dicarboxylic acids ($\gamma = 0.02 \pm 0.01$
53 to $\gamma = 0.18 \pm 0.07$) and levoglucosan ($\gamma < 0.01$ to $\gamma = 0.13 \pm 0.03$) over a range of humidities. However,
54 there are currently no measurements of the HO₂ uptake coefficient onto SOA published in the literature.

55 Using the kinetic multi-layer model of aerosol surface and bulk chemistry (KM-SUB), Shiraiwa
56 et al. (2011) have shown that the bulk diffusion of a species within an aerosol matrix can have a large
57 impact on a measured uptake coefficient. Diffusion coefficients of a particular species within a particle
58 are related to the viscosity of that particle with larger diffusion coefficients in less viscous particles.
59 Traditionally, the relationship between viscosity and diffusion coefficients is given by the Stokes-
60 Einstein equation, although this relation was found to break down for concentrated solutions and
61 solutions near their glass transition temperature or humidity (Champion et al., 1997;Power et al., 2013).
62 Zhou et al. (2013) have also shown that the rate of heterogeneous reaction of particle-borne
63 benzo[a]pyrene (BaP) with ozone within SOA particles was strongly dependent upon the bulk
64 diffusivity of the SOA. Along the same lines, Steimer et al. (2015) and Steimer et al. (2014)
65 demonstrated a clear link between the ozonolysis rates of shikimic acid and the changing diffusivity in
66 the transition between liquid and glassy states. Previous measurements of both N₂O₅ uptake coefficients
67 and HO₂ uptake coefficients onto humic acid aerosol particles and N₂O₅ uptake coefficients onto



68 malonic acid and citric acid aerosol particles have shown much lower uptake coefficients at low relative
69 humidities compared to higher humidities (Badger et al., 2006;Thornton et al., 2003;Lakey et al.,
70 2015a;Gržinić et al., 2015). However, viscosity effects have not been investigated systematically for
71 HO₂ uptake, and the first aim of this paper was to investigate whether a change in aerosol viscosity,
72 exemplified using the well-studied model compound sucrose (Berkemeier et al., 2014;Price et al.,
73 2014;Zobrist et al., 2011), could impact the HO₂ uptake coefficient. The second aim of this study was
74 to measure the HO₂ uptake coefficient onto two different types of SOA representative of biogenic and
75 anthropogenic SOA. α -pinene is the major terpene that forms biogenic SOA, while 1,3,5-
76 trimethylbenzene (TMB) is representative of alkyl benzenes which are the most abundant aromatic
77 hydrocarbons and form anthropogenic SOA (Calvert et al., 2002;Qi et al., 2012). SOA is known to be
78 highly viscous with viscosities of $10^3 - 10^6$ Pa s at 50 % RH (Renbaum-Wolff et al., 2013).

79

80 2. Experimental

81

82 The general experimental setup for the Leeds aerosol flow tube and the data analysis
83 methodology to determine values of γ have previously been discussed in detail by George et al. (2013).
84 This is the same experimental setup and data analysis methodology that was used for the copper doped
85 sucrose experiments, which were also performed at the University of Leeds. Therefore, only a brief
86 description of the setup is included below, with the emphasis being on changes made to the apparatus
87 for the SOA experiments undertaken at the Paul Scherrer Institute (PSI), Switzerland, for which a
88 schematic is shown in Figure 1. For all experiments the HO₂ radical was released at the end of an
89 injector which was moved backwards and forwards along an aerosol flow tube. The flow from the
90 injector was 1.32 ± 0.05 slpm. For the copper doped sucrose experiments the humid aerosol flow was
91 1.0 ± 0.1 slpm, and was mixed with a much drier flow (with the humidity of this flow being controlled
92 by mixing a flow from a water bubbler with a dry flow in different ratios) of 3.0 ± 0.3 slpm within a
93 conditioning flow tube for approximately ten seconds before entering the aerosol flow tube. Nitrogen
94 was used for all of these flows. For the SOA experiments the flow from the smog chamber or Potential
95 Aerosol Mass (PAM) chamber at PSI was 4.0 ± 0.3 slpm. Decays of the HO₂ radical along an aerosol
96 flow tube were measured using a Fluorescence Assay by Gas Expansion (FAGE) detector in both the
97 absence and presence of different concentrations of aerosol particles. All experiments were performed
98 at room temperature (293 ± 2 K).

99 The HO₂ radical was formed via Reactions 1 – 2, by passing a humidified flow over a mercury
100 penray lamp (L.O.T. Oriel, model 6035) in the presence of trace amounts (20 – 30 ppm) of oxygen in
101 the nitrogen flow.



102



105

106 The HO₂ radicals entered the FAGE cell through a 0.7 mm diameter pinhole, and were then converted
107 to OH by reacting with added NO. The FAGE cell was either kept at a pressure of ~ 0.85 Torr or ~ 1.5
108 Torr using a combination of a rotary pump (Edwards, model E1M80) and a roots blower (EH1200).
109 The OH radicals were detected by laser induced fluorescence at 308 nm (Heard and Pilling, 2003; Stone
110 et al., 2012). Initial HO₂ concentrations (obtained by calibration) exiting the injector were measured as
111 ~ 1 × 10⁹ molecule cm⁻³ for all experiments (following mixing and dilution with the main flow), and the
112 concentration was then measured as a function of distance along the flow tube.

113 For the experiments using copper doped sucrose aerosol particles, 3.42 grams of sucrose
114 (Fisher, > 99%) and 0.125 grams of copper (II) sulphate pentahydrate were dissolved in 500 ml of
115 milliQ water. These solutions were then placed in an atomiser (TSI, 3076) in order to form aerosol
116 particles. The aerosol particles passed through a neutraliser (Grimm 5522) and an impactor before
117 entering the conditioning flow tube. The size distribution of the aerosol particles were then measured
118 at the end of the reaction flow tube using a Scanning Mobility Particle Sizer (SMPS, TSI, 3080).

119 The experimental setup used to measure previous HO₂ uptake coefficients (George et al.,
120 2013; Matthews et al., 2014; Lakey et al., 2015a; Lakey et al., 2015b) was transported from the University
121 of Leeds, UK, to the Paul Scherrer Institute, Switzerland, where it was connected to the Paul Scherrer
122 Institute (PSI) smog chamber and, for some of the experiments, also to a Potential Aerosol Mass (PAM)
123 chamber (see Figure 1). The PSI smog chamber has a volume of 27 cubic metres, it is made from 125
124 µm Teflon fluorocarbon film and has been described elsewhere (Paulsen et al., 2005). To initiate
125 photochemical reactions four 4 kW xenon arc lamps (light spectrum >280 nm, OSRAM) and eighty
126 black lights (100W tubes, light spectrum between 320 and 400 nm, Cleo Performance) were used. For
127 most experiments the chamber was first humidified to 50% relative humidity, but for two experiments
128 this was increased to 80%, after which the precursor gases were added. The concept, design and
129 operation of a PAM chamber has also previously been described (Kang et al., 2007). The PAM chamber
130 at PSI is a flow tube of 0.46 m in length and 0.22 m internal diameter. Two low pressure Hg lamps
131 mainly emitting at 185 and 254 nm produce ozone in the chamber. Water vapour was photolysed by the
132 185 nm radiation to produce OH and HO₂ and also photolysed O₂ to produce O₃, whereas the 254 nm
133 light could also photolyse O₃ to produce OH following the reaction of O(¹D) with water vapour. Upper-
134 limit OH production rates are in the range of 1 × 10¹² - 2 × 10¹² molecule cm⁻³ s⁻¹ (Bruns et al., 2015).
135 The composition and oxidation state of SOA formed within PAM chambers has previously been shown



136 to be similar to SOA generated within environmental chambers (Bruns et al., 2015; Lambe et al., 2011a)
137 and SOA in the atmosphere (Ortega et al., 2015).

138 Four different types of experiments were performed.

139 (i) α -pinene ozonolysis in the PSI smog chamber (600 ppb α -pinene, 280 ppb ozone: ozone was added
140 first to the chamber; after injection of α -pinene particle nucleation and growth rapidly occurred).

141 (ii) OH initiated α -pinene photochemistry in the smog chamber (500 ppb α -pinene, 350 ppb NO₂: Xenon
142 and black lights were used to initiate photochemical reactions).

143 (iii) OH initiated α -pinene photochemistry in the PAM chamber (500 ppb α -pinene was filled into the
144 large smog chamber at 50 or 80 % RH to supply a constant concentration of α -pinene to the PAM
145 chamber, all SOA was formed within the PAM chamber).

146 (iv) OH initiated TMB photochemistry in the PAM chamber (2 ppm TMB was filled into the large smog
147 chamber at 50 % RH to supply a constant concentration of TMB to the PAM chamber, all SOA was
148 formed within the PAM chamber).

149 These precursor concentrations were chosen in order to obtain a large enough aerosol surface
150 area in the flow tube to be able to measure a HO₂ uptake coefficient. Experiments were performed only
151 once the aerosol surface area within the aerosol flow tube exceeded $5 \times 10^{-5} \text{ cm}^2 \text{ cm}^{-3}$, and in the case
152 of the smog chamber experiments once a maximum aerosol concentration had been reached (as
153 summarised in Section 5.2). Prior to entering the flow tube, the aerosol flow from the smog or PAM
154 chamber (4.0 slpm) was passed through either two or three cobalt oxide denuders in series. Each
155 denuder consisted of a 40 cm long, 0.8 cm inner diameter quartz tube coated with cobalt oxide prepared
156 by thermal decomposition of a saturated Co(NO₃)₂ solution applied to its inner walls at 700°C, as
157 described in Ammann (2001). These denuders were placed in series with a charcoal denuder (length =
158 16.4 cm, diameter = 0.9 cm, 69 quadratic channels) in order to remove NO_x, RO₂, VOC's and ozone
159 that had been present in the chamber. These denuders have previously been shown to be extremely
160 efficient at removing gas phase NO_x and VOCs (Arens et al., 2001). It should be noted that the flows
161 were drawn through the aerosol flow tube using a pump instead of the normal procedure whereby the
162 flows are pushed through the experimental setup using mass flow controllers. The pumping setup led
163 to slightly reduced pressures (904 – 987 mbar) in the aerosol flow tube, and so careful checks were
164 performed to ensure that the flow tube was vacuum tight. The aerosol size distribution from which the
165 surface area exiting the flow tube was calculated was measured using a Scanning Mobility Particle Sizer
166 (SMPS), which consisted of a neutraliser (Kr-85), a Differential Mobility Analyser (DMA, length 93.5
167 cm, inner radius 0.937 cm and outer radius 1.961 cm) and a Condensation Particle Counter (CPC, TSI,
168 model 3775). A typical surface weighted aerosol size distribution for the α -pinene derived aerosol



169 particles is shown in Figure 2. Note that an impactor was not used in the experimental setup for the
170 SOA measurements as this restricted the flow that could be pumped through the flow tube and was also
171 found to be unnecessary as the aerosol size distribution from the chambers fell entirely within the range
172 of aerosol sizes that the SMPS could measure.

173 In order to check that the experimental setup used at PSI produced consistent results with those
174 previously performed at the University of Leeds, an experiment was performed with ammonium
175 sulphate aerosol particles. The ammonium sulphate aerosol particles were formed using an atomiser
176 rather than aerosol particles being formed in a chamber, but were then passed through the same set up
177 (including the denuders) as the SOA was passed through. The experiment was performed at a flow tube
178 pressure of 915 mbar, due to the flows being pumped through the setup, (compared to pressures of 904
179 – 987 mbar for the SOA experiments), and a HO₂ uptake coefficient of 0.004 ± 0.002 was measured at
180 60% RH which is in agreement with previous experiments by George et al. (2013), which were
181 performed at atmospheric pressure (~ 970 – 1040 mbar).

182

183 3. Data analysis

184

185 Experiments were performed by moving the HO₂ injector backwards and forwards along the
186 flow tube either in the presence of or in the absence of aerosol particles, and recording the FAGE signal
187 from HO₂ radicals. The background signal in the absence of HO₂ (mercury lamp in the injector switched
188 off), but with the NO entering the FAGE cell, was recorded and was subtracted, from the signal during
189 experiments. For α -pinene experiments this background signal was small and similar to previous
190 experiments using dust, organic and inorganic salt aerosol particles (George et al., 2013; Lakey et al.,
191 2015b; Lakey et al., 2015a; Matthews et al., 2014). However, for the TMB experiments this background
192 signal varied from about half to two thirds of the signal from HO₂ with the mercury lamp in the injector
193 switched on. The background signal disappeared when the NO added to the FAGE cell was switched
194 off showing that it was not due to OH. The background signal within experiments did not change when
195 aerosol particles were present compared to when they were completely filtered out (see Figure 1). Due
196 to the efficiency of the denuders at removing gas phase species (Arens et al., 2001) it can be
197 hypothesised that the signal was due to alkenes, outgassing from the TMB aerosol particles that were
198 trapped on the HEPA filter, which then reacted with trace amounts of O₃ forming both HO₂ and RO₂
199 radicals. RO₂ species would have been observed as a HO₂ interference by the FAGE detection method.
200 FAGE interferences have previously been observed for alkene, aromatic and > C₃ alkane derived RO₂
201 (Fuchs et al., 2011; Whalley et al., 2013). A box model was run, utilising chemistry within the Master
202 Chemical Mechanism (MCM 3.2), which is detailed further in Whalley et al. (2013)), and constrained



203 to the experimental concentrations, and showed that the expected interference from TMB RO₂ and α-
204 pinene RO₂ would have been equivalent to 0.59 × [HO₂] and 0.44 × [HO₂], respectively, at a NO flow
205 of 50 ml min⁻¹ into the FAGE cell, a FAGE pressure of 1.5 Torr and a flow through the FAGE pinhole
206 of 4.2 slpm. However, for α-pinene experiments the background signal did not change between the NO
207 being switched on and off with the mercury lamp switched off in the injector, indicating the absence of
208 interferences in the FAGE cell for these experiments, and suggesting that for the α-pinene experiments
209 negligible concentrations of RO₂ species were present in the flow tube. Nevertheless, for TMB
210 experiments the background was measured regularly throughout the experiment in order to subtract it
211 from the data since a significant background signal was observed.

212 HO₂ decays along the flow tube in the presence and absence of aerosol particles were measured
213 between ~ 10 and 18 seconds flow time after the point of injection to ensure thorough mixing. A
214 previous calculation showed that the flows should be fully mixed by ~ 7 seconds (George et al., 2013).
215 An example of the HO₂ decays in the presence and absence of aerosol particles for a TMB experiment
216 is shown in Figure 3, plotted as the natural logarithm of HO₂ signal (proportional to concentration)
217 against reaction time according to:

$$\ln \frac{[HO_2]_t}{[HO_2]_0} = -k_{obs}t \quad (E1)$$

218 There is clear uptake of HO₂ observed by the SOA derived from TMB. The pseudo first-order
219 rate coefficients (k_{obs}) were then corrected to take into account wall loss and the non-plug flow
220 conditions using the methodology described by Brown (1978). These corrected rate constants (k') were
221 related to the HO₂ uptake coefficient (γ_{obs}) by the following equation:

$$k' = \frac{\gamma_{obs}\omega_{HO_2}S}{4} \quad (E2)$$

222 where ω_{HO_2} is the molecular thermal speed of HO₂ and S is the total aerosol surface area. Examples of
223 k' as a function of the aerosol surface area is shown in Figure 4. The HO₂ uptake coefficients were then
224 corrected for gas-phase diffusion limitations using the methodology described by (Fuchs and Sutugin,
225 1970), although this correction changed the uptake coefficient by less than 1 % for all experiments.

226

227 4. Model description

228

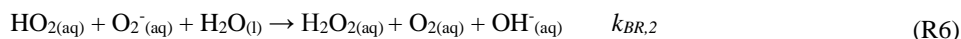
229 The kinetic multi-layer model of aerosol surface and bulk chemistry (KM-SUB) has been
230 described in detail by Shiraiwa et al. (2010). It is a multi-layer model comprising a gas phase, a near-
231 surface gas phase, a sorption layer, a near-surface bulk layer and a number of bulk layers. Processes



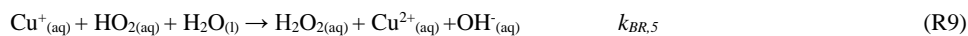
232 that can occur within the model include gas-phase diffusion, adsorption and desorption, bulk diffusion,
 233 and chemical reactions in the gas phase, at the surface and in the bulk. Input parameters to the model
 234 are summarised in Table 1 whilst the reactions that were included are shown below:



235



236



237

238 The bulk layer number was set to 100 corresponding to a bulk layer thickness of 0.5 nm which is only
 239 slightly larger than the diameter of HO₂ (0.4 nm). With this number of bulk layers the numerical model
 240 output of the HO₂ uptake coefficient converged such that increasing the number of layers further did
 241 not significantly impact the result. During experiments the average radius was observed to change by
 242 less than 10 % over the range of humidities, and therefore an assumption was made within the model
 243 that the average aerosol radius remained constant over the range of relative humidities. For the diffusion
 244 coefficient of HO₂ within aerosol particles, the measured diffusion coefficients of H₂O within sucrose
 245 solutions were used, which we then corrected using the Stokes-Einstein equation to take into account
 246 the larger radius of HO₂ radicals compared to H₂O molecules (Price et al., 2014; Zobrist et al., 2011).
 247 The correction resulted in a factor of 1.22 decrease in the diffusion coefficients of HO₂ compared to the
 248 diffusion coefficients of H₂O. It should be noted that above a viscosity of 10 Pa s the Stokes-Einstein
 249 relationship starts to fail and that the effect of increasing molecular size may become much stronger
 250 (Power et al., 2013). Price et al. (2014) estimated diffusion coefficients of H₂O by using Raman
 251 spectroscopy to observe D₂O diffusion in high-viscosity sucrose solutions whilst Zobrist et al. (2011)
 252 used optical techniques to observe changes in the size of sucrose particles when exposed to different
 253 relative humidities.

254



255 **5. Results and Discussion**

256

257 **5.1. HO₂ uptake by copper doped sucrose aerosol particles**

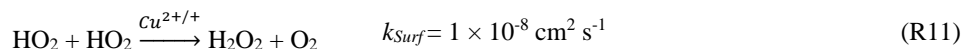
258

259 The results of the HO₂ uptake coefficient measurements onto copper doped sucrose aerosol
260 particles as a function of relative humidity (RH) are shown in Figure 5. The results show a large
261 dependence upon relative humidity with the HO₂ uptake coefficient increasing from $\gamma = 0.012 \pm 0.007$
262 at 17 ± 2 % RH to $\gamma = 0.22 \pm 0.06$ at relative humidities above 65%. The latter value is likely equal to
263 the surface accommodation coefficient, $\alpha_{s,0}$, and is consistent with many previous studies (Takahama
264 and Russell, 2011;George et al., 2013;Lakey et al., 2015b). At lower humidities, the diffusion
265 coefficients decrease which leads to a lower concentration of HO₂ within the bulk, and therefore to a
266 slower rate of HO₂ destruction (Reactions 7 – 10). The red and blue lines in

267 Figure 5 show the predicted HO₂ uptake coefficients using the KM-SUB model when using two
268 different parameterisations for HO₂ diffusion coefficients as a function of RH (see the model
269 description). There is good agreement between the model and the measurements suggesting that the
270 change in HO₂ uptake over the range of humidities is indeed due to a change in the HO₂ diffusion
271 coefficient which is in turn due to a change in the viscosity of the aerosol particles. Sensitivity tests
272 showed that an increase in the rate constants of reactions R7 – R10 would not affect the HO₂ uptake
273 coefficient whereas at the lower relative humidities with $\gamma < \alpha_{s,0}$ an increase in both the Henry's law
274 constant and diffusion coefficient increased the HO₂ uptake coefficient. The Henry's law constant and
275 HO₂ diffusion coefficient are both terms contained within the HO₂ bulk accommodation parameter
276 within the model suggesting that the uptake coefficient is limited by bulk accommodation at the lower
277 relative humidities (Berkemeier et al., 2013). At low relative humidities the HO₂ uptake coefficient was
278 also limited by chemical reaction at the surface (see the discussion below) (Berkemeier et al., 2013).

279 Although there is agreement between the measurements and model outputs for most of the data,
280 a surface reaction was required in order to obtain a good agreement between the model output and the
281 measured HO₂ uptake coefficient at low relative humidities. For example, at 17 % RH and without a
282 surface reaction, γ was estimated as $\sim 5 \times 10^{-4}$ and $\sim 3 \times 10^{-5}$ using the Zobrist et al. (2011) and Price et
283 al. (2014) parameterisations, respectively. However, by including the following reaction at the surface
284 of the sucrose particles, a much better agreement could be obtained:

285





286 The large rate constant for this reaction suggests that copper could potentially be catalysing the
287 destruction of HO₂ at the surface of the sucrose particles which is consistent with the higher HO₂ uptake
288 coefficients measured onto solid aerosol particles containing transition metals compared to solid aerosol
289 particles containing no transition metal ions (Matthews et al., 2014; Lakey et al., 2015a; Bedjanian et al.,
290 2013; George et al., 2013). A second potential reason also exists for the discrepancy at low humidities.
291 There could be incomplete equilibration of the aerosol particles with respect to RH, as they had only
292 been mixed with the conditioning flow for ~ 10 seconds before entering the reaction flow tube. Bones
293 et al. (2012) measured that for 100 nm diameter sucrose aerosol particles the equilibration time was
294 more than 10 seconds when the viscosity increased above ~ 10⁵ Pa s, which would occur at ~ 43 % RH
295 (Power et al., 2013). The actual diffusion coefficients would thus be higher than assumed in calculations
296 which assume fully equilibrated particles. However, the near-surface bulk of the aerosol particles, where
297 the reactions occur, would be much better equilibrated with respect to RH than the inner core of the
298 aerosol particles (Berkemeier et al., 2014). This means that the lack of aerosol equilibration with respect
299 to RH is likely to have a negligible impact upon the HO₂ uptake coefficient.

300 It should also be noted that the KM-SUB modelling results were very sensitive to the initial
301 aerosol pH. For example, at a pH of 4.1 (used in

302 Figure 5, the reason for this value is discussed below) the HO₂ uptake coefficient as predicted
303 by the KM-SUB model at 50 % RH (using the Zobrist et al. (2011) H₂O diffusion coefficients) was $\gamma =$
304 0.06 compared to $\gamma = 0.11$ at pH 5 and $\gamma = 0.21$ at pH 7. The reason for this strong dependence upon pH
305 has been discussed previously and is due to the partitioning of HO₂ with its conjugate base O₂⁻, as shown
306 by Reaction 4, affecting the effective Henry's law coefficient and the effective rate constants (Thornton
307 et al., 2008). Although it was not possible to measure the actual pH of the aerosol particles, it was
308 possible to estimate the concentration of copper (II) sulphate (which is a weak acid) within the aerosol
309 particles using the known growth factors of sucrose aerosol particles (Lu et al., 2014). The pH of 0.05
310 M and 0.1 M copper (II) sulphate solutions (which were calculated to be the extremes of the possible
311 copper concentrations over the RH range) were then measured using a pH meter (Jenway, 3310) as
312 being in the range of 4.10 ± 0.05. Therefore, there is confidence that the correct initial aerosol pH was
313 inputted into the model. Hence, while the HO₂ uptake coefficient might depend on further factors such
314 as aerosol pH, a clear dependence on relative humidity, and hence particle viscosity could be observed,
315 and it remains likely that at low humidity a surface loss process becomes dominating.

316

317

318



319 **5.2. HO₂ uptake by Secondary Organic Aerosol**

320

321 A summary of all HO₂ uptake experiments performed on SOA is shown in Table 2. On average
322 the HO₂ uptake coefficient was measured as $\gamma = 0.004 \pm 0.002$ onto TMB derived aerosol particles
323 produced in the PAM chamber, whereas for α -pinene derived aerosol particles only an upper limit of
324 $\gamma = 0.001$ (obtained from the error in the slope of Figure 4(a)) could be placed on the HO₂ uptake
325 coefficient at 50 and 80 % RH. It should be noted that for the α -pinene experiments the HO₂ uptake
326 coefficient was non-measurable for both ozonolysis and photochemistry experiments using both the
327 smog chamber and the PAM chamber as sources of the SOA, and therefore only upper limits of
328 individual experiments are reported in Table 2. There was some variability for the upper limits that
329 were measured for individual α -pinene experiments which is likely to be due to the maximum aerosol
330 surface-to-volume ratio that was obtained in each experiment.

331 There are several possible reasons for the larger HO₂ uptake coefficients being measured for
332 the TMB derived aerosol particles compared to the α -pinene derived aerosol particles. These reasons
333 will be summarised below, but include a differing particle viscosity, a different particle liquid water
334 content or a HO₂ + RO₂ reaction occurring within the aerosol particles. Although the viscosity of α -
335 pinene derived aerosol has been measured as $\sim 10^3$ Pa s at 70 % RH and $> 10^9$ Pa s for RH < 30 %, to
336 our knowledge, there are currently no measurements of the viscosity of TMB derived aerosol published
337 in the literature (Renbaum-Wolff et al., 2013). By running the KM-SUB model it can be estimated that
338 the diffusion coefficient of HO₂ within the particles would need to be approximately 1×10^{-10} cm² s⁻¹ for
339 TMB derived aerosol particles and $< 5 \times 10^{-12}$ cm² s⁻¹ for α -pinene derived aerosol particles. This range
340 of values seems to be consistent with the diffusion coefficients estimated by Berkemeier et al. (2014)
341 and Lienhard et al. (2015) for water diffusion in low and medium O:C SOA.

342 Thornton et al. (2003) previously suggested that for malonic acid aerosol particles the liquid
343 water content could be limiting the aqueous chemistry below 40 % RH. As can be seen by the HO₂
344 reaction scheme, the rate of Reaction R6 is dependent upon the liquid water concentration within the
345 aerosol, and therefore the uptake coefficient could be limited by a low aerosol liquid water content.
346 However, there remains some uncertainty as to whether the liquid water content of TMB derived aerosol
347 particles would be higher than the liquid water content of α -pinene derived aerosol particles. Duplissy
348 et al. (2011) measured a higher hygroscopicity parameter (κ_{org}) for TMB derived aerosol particles
349 compared to α -pinene derived aerosol particles whereas Lambe et al. (2011b) and Berkemeier et al.
350 (2014) stated the opposite. However, as well as being dependent upon the hygroscopicity parameter,
351 the liquid water content of the aerosol particles would also be dependent upon the O:C ratio in the SOA.



352 If the viscosity and liquid water content of the α -pinene and TMB derived aerosol particles are
353 similar, the larger HO₂ uptake coefficients measured for TMB derived aerosol particles could be due to
354 a higher reactivity of these aerosol particles towards HO₂. This could be the case if the TMB derived
355 aerosol particles contained reactive radical species such as organic peroxy radicals, RO₂, which partition
356 into the aerosol or are formed within the aerosols by intra-particular reactions (Donahue et al., 2012; Lee
357 et al., 2016). As previously stated in Section 3, during α -pinene experiments, no indication of RO₂ being
358 present in the flow tube was observed by FAGE as a HO₂ interference. However, for TMB derived
359 aerosol particles, a large background signal was observed by FAGE indicating that reactive radical
360 species were likely to be present within the flow tube. If the reaction of HO₂ with these species at the
361 surface or within the bulk of the aerosol was faster than the equivalent gas phase reaction, a larger HO₂
362 uptake coefficient would be observed.

363

364 **6. Atmospheric implications and conclusions**

365

366 The effect of aerosol viscosity upon HO₂ uptake coefficients was systematically investigated
367 with a combination of HO₂ uptake coefficient measurements and a state-of-the-art kinetic model. A
368 good correlation was obtained between measured HO₂ uptake coefficients onto copper doped sucrose
369 aerosols as a function of RH and the KM-SUB model output. The decrease in the HO₂ uptake coefficient
370 towards lower relative humidities suggests that lower diffusion coefficients lead to less HO₂ within the
371 bulk of the aerosol, and therefore to a decrease in the rate of HO₂ destruction. These results imply that
372 viscous aerosol particles will have very little impact upon gaseous tropospheric HO₂ concentrations.

373 The first measurements of the HO₂ uptake coefficient onto SOA have been reported in this
374 work. The HO₂ uptake coefficient measured for α -pinene derived aerosol particles was below the limit
375 of detection of the apparatus ($\gamma < 0.001$) whereas for TMB derived aerosol particles the uptake
376 coefficient was measurable ($\gamma = 0.004 \pm 0.002$). These results are consistent with the copper doped
377 sucrose results, and indicate that the impact of SOA on gaseous HO₂ concentrations would likely be
378 small. However, it remains unclear as to the reasons for the larger HO₂ uptake coefficient measured
379 onto TMB derived aerosol particles compared to α -pinene derived aerosol particles. The possibility that
380 the larger uptake coefficient onto TMB derived aerosol particles was due to a lower viscosity of the
381 aerosol particles or a higher liquid water content compared to α -pinene derived aerosol particles cannot
382 be confirmed until further measurements of the viscosity and liquid water content of TMB derived
383 aerosol particles are published in the literature. However, if the larger uptake coefficients are due to a
384 HO₂ + RO₂ reaction within the aerosol, this could impact the HO₂ uptake coefficient for any aerosol
385 containing RO₂. The actual increase would depend on a variety of factors such as the concentrations of



386 RO₂, the partition coefficients of RO₂ to the aerosol particles, the reactivity of different RO₂ species
387 with HO₂ radicals and the intra-particle formation of RO₂ and other reactive radicals (Lee et al.,
388 2016; Donahue et al., 2012; Tong et al., 2016). The HO₂ + RO₂ reaction could potentially occur within
389 the majority of aerosol particles within the atmosphere, this could have implications for the gaseous
390 HO₂ and RO₂ concentrations in the troposphere which could then impact upon the concentrations of
391 other species such as ozone.

392

393 **Acknowledgements**

394

395 PSJL is grateful to the UK National Environment Research Council (NERC) for the award of a
396 studentship. LKW and DEH are also grateful to the NERC funded National Centre for Atmospheric
397 Science for ongoing support and to NERC for funding of the HO₂ aerosol uptake apparatus (grant
398 reference NE/F020651/1). TB was supported by the Max Planck Graduate Centre with the Johannes
399 Gutenberg-Universität Mainz (MPGC). The experiments at PSI were supported by T. Bartels-Rausch
400 and M. Birrer. MA and MK were supported by the Swiss National Science Foundation (grant numbers
401 149492, CR3213-140851).

402

403

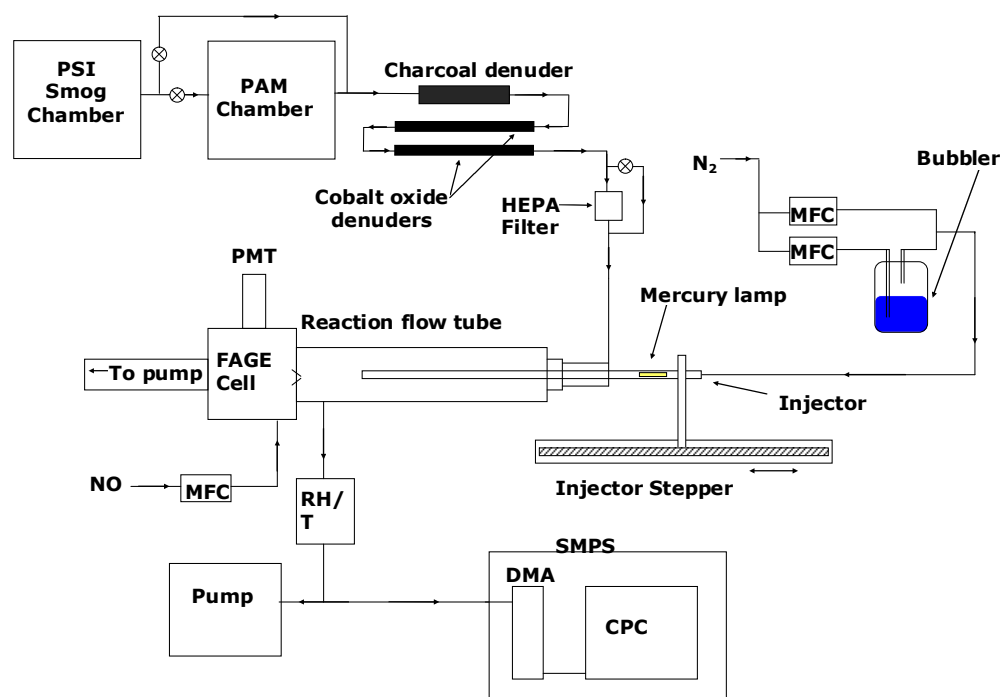
404

405

406



407 **Figures**



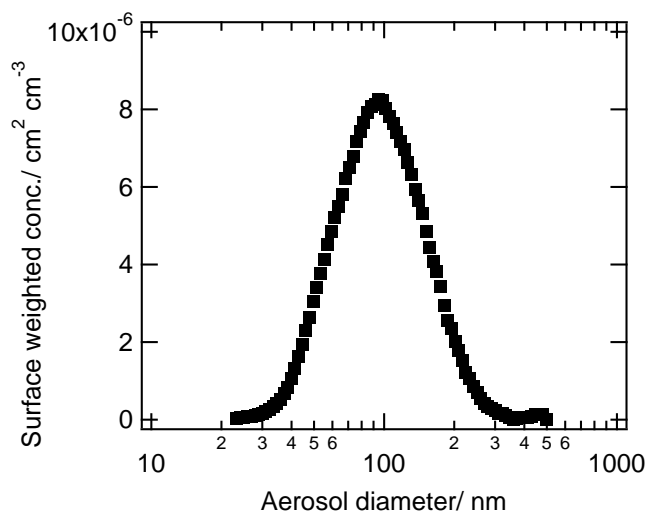
408

409

410 **Figure 1:** A schematic of the experimental setup used to measure HO₂ uptake coefficients onto SOA
411 aerosol particles. Key: PAM- Potential aerosol mass, PMT- Photomultiplier tube, FAGE- Fluorescence
412 Assay by Gas Expansion, MFC- Mass flow controller, RH/ T- relative humidity and temperature probe,
413 SMPS- Scanning mobility particle sizer, DMA- Differential mobility analyser, CPC- Condensation
414 particle counter.
415

416

417



418

419

420 **Figure 2:** An example of the size distribution for α -pinene derived aerosol particles formed in the
421 PAM chamber at a relative humidity of ~ 50 %.

422

423

424

425

426

427

428

429

430

431

432

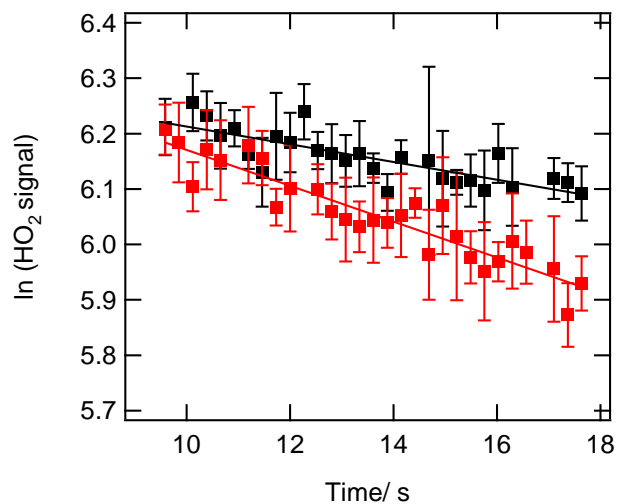
433

434

435

436

437



438

439

440 **Figure 3:** Examples of the HO₂ wall loss without any aerosol particles along the flow tube (black
441 squares) and the HO₂ loss with an aerosol surface area of $2.2 \times 10^{-4} \text{ cm}^2 \text{ cm}^{-3}$ for TMB derived aerosol
442 particles at an initial HO₂ concentration of $\sim 1 \times 10^9 \text{ molecule cm}^{-3}$ (red squares) and for RH = 50 %.
443 The error bars represent one standard deviation in the measured HO₂ signal for a measurement time per
444 point of 3 seconds.

445

446

447

448

449

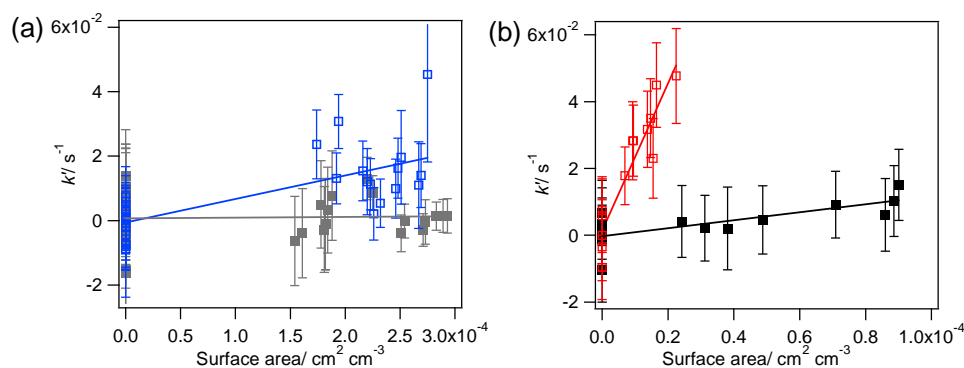
450

451

452

453

454



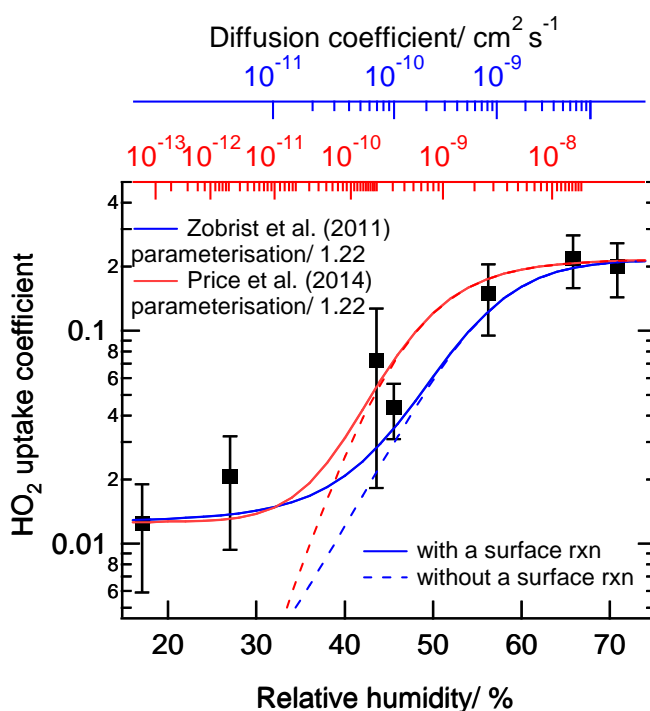
455

456

457 **Figure 4:** The pseudo-first-order rate constants with the wall losses subtracted as a function of aerosol
458 surface area for (a) α -pinene derived aerosol particles (grey) and TMB derived aerosol particles (blue)
459 at 50 % RH and a pressure of 904 – 929 mbar and (b) copper doped sucrose aerosol particles at 17%
460 RH (black) and 71% RH (red) at atmospheric pressure. Experiments were performed at 293 ± 2 K. In
461 panel (a) experiments were performed using the PAM chamber as the source of aerosol particles and
462 represent experiments 5 and 6 in Table 2. Error bars represent the 1 standard deviation propagated
463 uncertainty for individual determinations of k' . The data points at an aerosol surface area of $0 \text{ cm}^2 \text{ cm}^{-3}$
464 (no aerosol particles present) are repeats of the wall loss decays taken throughout the experiment and
465 are within error of each other.
466



467



468

469

470 **Figure 5:** The HO₂ uptake coefficient onto copper doped sucrose aerosol particles as a function of
471 relative humidity. The lines represent the expected HO₂ uptake coefficient calculated using the KM-
472 SUB model using the Price et al. (2014) (red) and Zobrist et al. (2011) (blue) diffusion parameterisations
473 (see Section 4) and with (solid) and without (dashed) the inclusion of a surface reaction (Reaction R11).
474 The error bars represent two standard deviations of the propagated error in the gradient of the k' against
475 aerosol surface area graphs. Please see text for more information about experimental conditions.
476

477

478

479

480

481

482

483

484

485 **Tables**

486

487 **Table 1:** The initial parameters used in the KM-SUB HO₂ uptake model.

488

Parameter	Description	Value at 293 K	Reference
$k_{BR,1}$	Rate constant, R5	$1.3 \times 10^{-15} \text{ cm}^{-3} \text{ s}^{-1}$	Thornton et al. (2008)
$k_{BR,2}$	Rate constant, R6	$1.5 \times 10^{-13} \text{ cm}^{-3} \text{ s}^{-1}$	Thornton et al. (2008)
$k_{BR,3}$	Rate constant, R7	$1.7 \times 10^{-13} \text{ cm}^{-3} \text{ s}^{-1}$	Jacob (2000)
$k_{BR,4}$	Rate constant, R8	$1.3 \times 10^{-11} \text{ cm}^{-3} \text{ s}^{-1}$	Jacob (2000)
$k_{BR,5}$	Rate constant, R9	$2.5 \times 10^{-12} \text{ cm}^{-3} \text{ s}^{-1}$	Jacob (2000)
$k_{BR,6}$	Rate constant, R10	$1.6 \times 10^{-11} \text{ cm}^{-3} \text{ s}^{-1}$	Jacob (2000)
k_{GP}	Rate constant, R3	$3 \times 10^{-12} \text{ cm}^{-3} \text{ s}^{-1}$	Sander et al. (2003)
K_{eq}	Equilibrium constant, R4	$2.1 \times 10^{-5} \text{ M}$	Thornton et al. (2008)
H_{HO_2}	HO ₂ Henry's law constant	5600 M atm^{-1}	Thornton et al. (2008)
τ_d	HO ₂ desorption lifetime	$1.5 \times 10^{-3} \text{ s}$	Shiraiwa et al. (2010)
$\alpha_{s,0}$	HO ₂ surface accommodation at time 0	0.22	
D_{g,HO_2}	HO ₂ gas phase diffusion rate constant	$0.25 \text{ cm}^2 \text{ s}^{-1}$	Thornton et al. (2008)
[Cu]	Copper concentration (used when modelling copper doped sucrose aerosol particles)	$2 \times 10^{20} \text{ cm}^{-3}$	
T	Temperature	293 K	

489

490

491

492

493

494

495



496 **Table 2:** Summary of the reactants and conditions that were utilised and the HO₂ uptake coefficients
 497 that were measured during the experiments. Experiments 1 - 4 were performed using the smog
 498 chamber whereas experiments 5 - 9 utilised the PAM chamber.
 499

Experiment number	Reaction type	Initial precursor concentrations	UV	Relative humidity in the chamber/%	Pressure in the flow tube/mbar	Maximum aerosol surface to volume ratio in the flow tube/cm ² cm ⁻³	HO ₂ uptake coefficient (γ)
1	α-pinene ozonolysis	[α-pinene] = 600 ppb [O ₃] = 280 ppb	Off	50	987	6.30 × 10 ⁻⁵	< 0.01
2	α-pinene ozonolysis	[α-pinene] = 600 ppb [O ₃] = 280 ppb	Off	50	965	1.30 × 10 ⁻⁴	< 0.004
3	α-pinene ozonolysis	[α-pinene] = 200 ppb [O ₃] = 310 ppb	Off	80	939	7.10 × 10 ⁻⁵	< 0.006
4	α-pinene photochemistry	[α-pinene] = 500 ppb [NO ₂] = 350 ppb	On	50	940	6.30 × 10 ⁻⁵	< 0.018
5	α-pinene photochemistry	[α-pinene] = 500 ppb	On	50	929	2.93 × 10 ⁻⁴	< 0.001
6	TMB photochemistry	[TMB] = 2 ppm	On	50	923	2.75 × 10 ⁻⁴	0.004 ± 0.002
7	TMB photochemistry	[TMB] = 2ppm	On	50	918	2.32 × 10 ⁻⁴	0.004 ± 0.003
8	α-pinene photochemistry	[α-pinene] = 500 ppb	On	50	927	1.88 × 10 ⁻⁴	< 0.005
9	α-pinene photochemistry	[α-pinene] = 1 ppm	On	80	904	3.90 × 10 ⁻⁴	< 0.001

500

501

502

503

504 **References**

- 505 Ammann, M.: Using ^{13}N as tracer in heterogeneous atmospheric chemistry experiments,
506 *Radiochimica Acta International journal for chemical aspects of nuclear science and technology*, 89,
507 831, 2001.
- 508 Arens, F., Gutzwiller, L., Baltensperger, U., Gäggeler, H. W., and Ammann, M.: Heterogeneous
509 reaction of NO_2 on diesel soot particles, *Environ. Sci. Technol.*, 35, 2191-2199, 2001.
- 510 Badger, C. L., Griffiths, P. T., George, I., Abbatt, J. P. D., and Cox, R. A.: Reactive uptake of N_2O_5
511 by aerosol particles containing mixtures of humic acid and ammonium sulfate, *J. Phys. Chem. A*, 110,
512 6986-6994, 10.1021/jp0562678, 2006.
- 513 Bedjanian, Y., Romanias, M. N., and El Zein, A.: Uptake of HO_2 radicals on Arizona Test Dust,
514 *Atmos. Chem. Phys.*, 6461-6471, 2013.
- 515 Berkemeier, T., Huisman, A. J., Ammann, M., Shiraiwa, M., Koop, T., and Pöschl, U.: Kinetic
516 regimes and limiting cases of gas uptake and heterogeneous reactions in atmospheric aerosols and
517 clouds: a general classification scheme, *Atmos. Chem. Phys. Discuss.*, 13, 983-1044, 10.5194/acp-
518 13-983-2013, 2013.
- 519 Berkemeier, T., Shiraiwa, M., Pöschl, U., and Koop, T.: Competition between water uptake and ice
520 nucleation by glassy organic aerosol particles, *Atmos. Chem. Phys.*, 14, 12513-12531, 2014.
- 521 Bones, D. L., Reid, J. P., Lienhard, D. M., and Krieger, U. K.: Comparing the mechanism of water
522 condensation and evaporation in glassy aerosol, *P. Natl. Acad. Sci.*, 109, 11613-11618,
523 10.1073/pnas.1200691109, 2012.
- 524 Brown, R. L.: Tubular Flow Reactors With 1st-Order Kinetics, *J. Res. Nat. Bur. Stand.*, 83, 1-8,
525 1978.
- 526 Bruns, E., El Haddad, I., Keller, A., Klein, F., Kumar, N., Pieber, S., Corbin, J., Slowik, J., Brune, W.,
527 and Baltensperger, U.: Inter-comparison of laboratory smog chamber and flow reactor systems on
528 organic aerosol yield and composition, *Atmospheric Measurement Techniques*, 8, 2315-2332, 2015.
- 529 Calvert, J. G., Atkinson, R., Becker, K. H., Kamens, R. M., Seinfeld, J. H., Wallington, T. J., and
530 Yarwood, G.: *The Mechanisms of Atmospheric Oxidation of Aromatic Hydrocarbons*, Oxford
531 University Press, Oxford, 2002.
- 532 Champion, D., Hervet, H., Blond, G., Le Meste, M., and Simatos, D.: Translational diffusion in
533 sucrose solutions in the vicinity of their glass transition temperature, *J. Phys. Chem. B*, 101, 10674-
534 10679, 1997.
- 535 Donahue, N. M., Henry, K. M., Mentel, T. F., Kiendler-Scharr, A., Spindler, C., Bohn, B., Brauers,
536 T., Dorn, H. P., Fuchs, H., and Tillmann, R.: Aging of biogenic secondary organic aerosol via gas-
537 phase OH radical reactions, *P. Natl. Acad. Sci.*, 109, 13503-13508, 2012.
- 538 Duplissy, J., DeCarlo, P. F., Dommen, J., Alfarra, M. R., Metzger, A., Barmapadimos, I., Prevot, A. S.
539 H., Weingartner, E., Tritscher, T., Gysel, M., Aiken, A. C., Jimenez, J. L., Canagaratna, M. R.,
540 Worsnop, D. R., Collins, D. R., Tomlinson, J., and Baltensperger, U.: Relating hygroscopicity and
541 composition of organic aerosol particulate matter, *Atmos. Chem. Phys.*, 11, 1155-1165, 10.5194/acp-
542 11-1155-2011, 2011.



- 543 Fowler, D., Pilegaard, K., Sutton, M., Ambus, P., Raivonen, M., Duyzer, J., Simpson, D., Fagerli, H.,
544 Fuzzi, S., and Schjørring, J. K.: Atmospheric composition change: ecosystems–atmosphere
545 interactions, *Atmos. Environ.*, 43, 5193–5267, 2009.
- 546 Fuchs, H., Bohn, B., Hofzumahaus, A., Holland, F., Lu, K. D., Nehr, S., Rohrer, F., and Wahner, A.:
547 Detection of HO₂ by laser-induced fluorescence: calibration and interferences from RO₂ radicals,
548 *Atmos. Meas. Tech.*, 4, 1209–1225, 10.5194/amt-4-1209-2011, 2011.
- 549 Fuchs, N. A., and Sutugin, A. G.: Properties of Highly Dispersed Aerosols, in, 1970.
- 550 George, I. J., Matthews, P. S. J., Whalley, L. K., Brooks, B., Goddard, A., Baeza-Romero, M. T., and
551 Heard, D. E.: Measurements of uptake coefficients for heterogeneous loss of HO₂ onto submicron
552 inorganic salt aerosols, *Phys. Chem. Chem. Phys.*, 15, 12829–12845, 10.1039/C3CP51831K, 2013.
- 553 Gržinić, G., Bartels-Rausch, T., Berkemeier, T., Türler, A., and Ammann, M.: Viscosity controls
554 humidity dependence of N₂O₅ uptake to citric acid aerosol, *Atmos. Chem. Phys.*, 15, 13615–13625,
555 2015.
- 556 Heard, D. E., and Pilling, M. J.: Measurement of OH and HO₂ in the troposphere, *Chem. Rev.*, 103,
557 5163–5198, 10.1021/cr020522s, 2003.
- 558 Jacob, D. J.: Heterogeneous chemistry and tropospheric ozone, *Atmos. Environ.*, 34, 2131–2159,
559 2000.
- 560 Kanakidou, M., Seinfeld, J. H., Pandis, S. N., Barnes, I., Dentener, F. J., Facchini, M. C., Van
561 Dingenen, R., Ervens, B., Nenes, A., Nielsen, C. J., Swietlicki, E., Putaud, J. P., Balkanski, Y., Fuzzi,
562 S., Horth, J., Moortgat, G. K., Winterhalter, R., Myhre, C. E. L., Tsigaridis, K., Vignati, E.,
563 Stephanou, E. G., and Wilson, J.: Organic aerosol and global climate modelling: a review, *Atmos.*
564 *Chem. Phys.*, 5, 1053–1123, 2005.
- 565 Kanaya, Y., Cao, R., Kato, S., Miyakawa, Y., Kajii, Y., Tanimoto, H., Yokouchi, Y., Mochida, M.,
566 Kawamura, K., and Akimoto, H.: Chemistry of OH and HO₂ radicals observed at Rishiri Island,
567 Japan, in September 2003: Missing daytime sink of HO₂ and positive nighttime correlations with
568 monoterpenes, *J. Geophys. Res. - Atmos.*, 112, D11308, 10.1029/2006jd007987, 2007.
- 569 Kang, E., Root, M. J., Toohey, D. W., and Brune, W. H.: Introducing the concept of Potential Aerosol
570 Mass (PAM), *Atmos. Chem. Phys.*, 7, 5727–5744, 2007.
- 571 Lakey, P. S. J., George, I. J., Whalley, L. K., Baeza-Romero, M. T., and Heard, D. E.: Measurements
572 of the HO₂ Uptake Coefficients onto Single Component Organic Aerosols, *Environ. Sci. Tech.*,
573 10.1021/acs.est.5b00948, 2015a.
- 574 Lakey, P. S. J., George, I. J., Baeza-Romero, M. T., Whalley, L. K., and Heard, D. E.: Organics
575 substantially reduce HO₂ uptake onto aerosols containing transition metal ions, *J. Phys Chem. A*,
576 2015b.
- 577 Lambe, A., Ahern, A., Williams, L., Slowik, J., Wong, J., Abbatt, J., Brune, W., Ng, N., Wright, J.,
578 and Croasdale, D.: Characterization of aerosol photooxidation flow reactors: heterogeneous oxidation,
579 secondary organic aerosol formation and cloud condensation nuclei activity measurements,
580 *Atmospheric Measurement Techniques*, 4, 445–461, 2011a.
- 581 Lambe, A. T., Onasch, T. B., Massoli, P., Croasdale, D. R., Wright, J. P., Ahern, A. T., Williams, L.
582 R., Worsnop, D. R., Brune, W. H., and Davidovits, P.: Laboratory studies of the chemical
583 composition and cloud condensation nuclei (CCN) activity of secondary organic aerosol (SOA) and



- 584 oxidized primary organic aerosol (OPOA), Atmos. Chem. Phys., 11, 8913-8928, 10.5194/acp-11-
585 8913-2011, 2011b.
- 586 Lee, B. H., Mohr, C., Lopez-Hilfiker, F. D., Lutz, A., Hallquist, M., Lee, L., Romer, P., Cohen, R. C.,
587 Iyer, S., and Kurtén, T.: Highly functionalized organic nitrates in the southeast United States:
588 Contribution to secondary organic aerosol and reactive nitrogen budgets, P. Natl. Acad. Sci., 113,
589 1516-1521, 2016.
- 590 Lienhard, D., Huisman, A., Krieger, U., Rudich, Y., Marcolli, C., Luo, B., Bones, D., Reid, J., Lambe,
591 A., and Canagaratna, M.: Viscous organic aerosol particles in the upper troposphere: diffusivity-
592 controlled water uptake and ice nucleation?, Atmos. Chem. Phys., 15, 13599-13613, 2015.
- 593 Lim, H. J., and Turpin, B. J.: Origins of primary and secondary organic aerosol in Atlanta: Results' of
594 time-resolved measurements during the Atlanta supersite experiment, Environ. Sci. Technol., 36,
595 4489-4496, 10.1021/es0206487, 2002.
- 596 Lu, J. W., Rickards, A. M., Walker, J. S., Knox, K. J., Miles, R. E., Reid, J. P., and Signorell, R.:
597 Timescales of water transport in viscous aerosol: measurements on sub-micron particles and
598 dependence on conditioning history, Phys. Chem. Chem. Phys., 16, 9819-9830, 10.1039/c3cp54233e,
599 2014.
- 600 Mao, J., Jacob, D. J., Evans, M. J., Olson, J. R., Ren, X., Brune, W. H., St Clair, J. M., Crounse, J. D.,
601 Spencer, K. M., Beaver, M. R., Wennberg, P. O., Cubison, M. J., Jimenez, J. L., Fried, A., Weibring,
602 P., Walega, J. G., Hall, S. R., Weinheimer, A. J., Cohen, R. C., Chen, G., Crawford, J. H.,
603 McNaughton, C., Clarke, A. D., Jaegle, L., Fisher, J. A., Yantosca, R. M., Le Sager, P., and Carouge,
604 C.: Chemistry of hydrogen oxide radicals (HO_x) in the Arctic troposphere in spring, Atmos. Chem.
605 Phys., 10, 5823-5838, 10.5194/acp-10-5823-2010, 2010.
- 606 Matthews, P. S. J., Baeza-Romero, M. T., Whalley, L. K., and Heard, D. E.: Uptake of HO₂ radicals
607 onto Arizona test dust particles using an aerosol flow tube, Atmos. Chem. Phys., 14, 7397-7408,
608 10.5194/acpd-14-4229-2014, 2014.
- 609 Ortega, A. M., Hayes, P. L., Peng, Z., Palm, B. B., Hu, W., Day, D. A., Li, R., Cubison, M. J., Brune,
610 W. H., Graus, M., Warneke, C., Gilman, J. B., Kuster, W. C., de Gouw, J. A., and Jimenez, J. L.:
611 Real-time measurements of secondary organic aerosol formation and aging from ambient air in an
612 oxidation flow reactor in the Los Angeles area, Atmos. Chem. Phys. Discuss., 2015, 21907-21958,
613 10.5194/acpd-15-21907-2015, 2015.
- 614 Paulsen, D., Dommen, J., Kalberer, M., Prévôt, A. S. H., Richter, R., Sax, M., Steinbacher, M.,
615 Weingartner, E., and Baltensperger, U.: Secondary Organic Aerosol Formation by Irradiation of 1,3,5-
616 Trimethylbenzene-NO_x-H₂O in a New Reaction Chamber for Atmospheric Chemistry and Physics,
617 Environ. Sci. Technol., 39, 2668-2678, 10.1021/es0489137, 2005.
- 618 Pöschl, U., and Shiraiwa, M.: Multiphase Chemistry at the Atmosphere-Biosphere Interface
619 Influencing Climate and Public Health in the Anthropocene, Chem. Rev., 115, 4440-4475, 2015.
- 620 Power, R. M., Simpson, S. H., Reid, J. P., and Hudson, A. J.: The transition from liquid to solid-like
621 behaviour in ultrahigh viscosity aerosol particles, Chem. Sci., 4, 2597-2604, 10.1039/C3SC50682G,
622 2013.
- 623 Price, H. C., Murray, B. J., Mattsson, J., O'Sullivan, D., Wilson, T. W., Baustian, K. J., and Benning,
624 L. G.: Quantifying water diffusion in high-viscosity and glassy aqueous solutions using a Raman
625 isotope tracer method, Atmos. Chem. Phys., 14, 3817-3830, 10.5194/acpd-13-29375-2013, 2014.



- 626 Qi, L., Nakao, S., and Cocker III, D. R.: Aging of secondary organic aerosol from α -pinene
627 ozonolysis: Roles of hydroxyl and nitrate radicals, *J. Air Waste Manage.*, 62, 1359-1369, 2012.
- 628 Renbaum-Wolff, L., Grayson, J. W., Bateman, A. P., Kuwata, M., Sellier, M., Murray, B. J., Shilling,
629 J. E., Martin, S. T., and Bertram, A. K.: Viscosity of alpha-pinene secondary organic material and
630 implications for particle growth and reactivity, *P. Natl. Acad. Sci.*, 110, 8014-8019,
631 10.1073/pnas.1219548110, 2013.
- 632 Sander, S. P., Friedl, R. R., Golden, D. M., Kurylo, M. J., Huie, R. E., Orkin, V. L., Moortgat, G. K.,
633 Ravishankara, A. R., Kolb, C. E., Molina, M. J., and Finlayson-Pitts, B. J.: Chemical Kinetics and
634 Photochemical Data for Use in Atmospheric Studies, JPL Publication, 14, 2003.
- 635 Shiraiwa, M., Pfrang, C., and Pöschl, U.: Kinetic multi-layer model of aerosol surface and bulk
636 chemistry (KM-SUB): the influence of interfacial transport and bulk diffusion on the oxidation of
637 oleic acid by ozone, *Atmos. Chem. Phys.*, 10, 3673-3691, 10.5194/acp-10-3673-2010, 2010.
- 638 Shiraiwa, M., Ammann, M., Koop, T., and Pöschl, U.: Gas uptake and chemical aging of semisolid
639 organic aerosol particles, *P. Natl. Acad. Sci.*, 108, 11003-11008, 2011.
- 640 Steimer, S., Lampimäki, M., Coz, E., Grzinic, G., and Ammann, M.: The influence of physical state
641 on shikimic acid ozonolysis: a case for in situ microspectroscopy, *Atmos. Chem. Phys.*, 14, 10761-
642 10772, 2014.
- 643 Steimer, S. S., Berkemeier, T., Gilgen, A., Krieger, U. K., Peter, T., Shiraiwa, M., and Ammann, M.:
644 Shikimic acid ozonolysis kinetics of the transition from liquid aqueous solution to highly viscous
645 glass, *Phys. Chem. Chem. Phys.*, 2015.
- 646 Stone, D., Whalley, L. K., and Heard, D. E.: Tropospheric OH and HO₂ radicals: field measurements
647 and model comparisons, *Chemical Society Reviews*, 41, 6348-6404, 10.1039/c2cs35140d, 2012.
- 648 Takahama, S., and Russell, L.: A molecular dynamics study of water mass accommodation on
649 condensed phase water coated by fatty acid monolayers, *J. Geophys. Res. - Atmos.*, 116, 2011.
- 650 Taketani, F., and Kanaya, Y.: Kinetics of HO₂ Uptake in Levoglucosan and Polystyrene Latex
651 Particles, *Journal of Physical Chemistry Letters*, 1, 1701-1704, 10.1021/jz100478s, 2010.
- 652 Taketani, F., Kanaya, Y., and Akimoto, H.: Kinetic Studies of Heterogeneous Reaction of HO₂
653 Radical by Dicarboxylic Acid Particles, *International Journal of Chemical Kinetics*, 45, 560-565,
654 10.1002/kin.20783, 2013.
- 655 Thornton, J. A., Braban, C. F., and Abbatt, J. P. D.: N₂O₅ hydrolysis on sub-micron organic aerosols:
656 the effect of relative humidity, particle phase, and particle size, *Phys. Chem. Chem. Phys.*, 5, 4593-
657 4603, 10.1039/B307498F, 2003.
- 658 Thornton, J. A., Jaegle, L., and McNeill, V. F.: Assessing known pathways for HO₂ loss in aqueous
659 atmospheric aerosols: Regional and global impacts on tropospheric oxidants, *J. Geophys. Res. -
660 Atmos.*, 113, D05303, 10.1029/2007jd009236, 2008.
- 661 Tong, H., Arangio, A. M., Lakey, P. S. J., Berkemeier, T., Liu, F., Kampf, C. J., Brune, W. H.,
662 Pöschl, U., and Shiraiwa, M.: Hydroxyl radicals from secondary organic aerosol decomposition in
663 water, *Atmos. Chem. Phys.*, 16, 1761-1771, 10.5194/acp-16-1761-2016, 2016.
- 664 Whalley, L. K., Furneaux, K. L., Goddard, A., Lee, J. D., Mahajan, A., Oetjen, H., Read, K. A.,
665 Kaaden, N., Carpenter, L. J., Lewis, A. C., Plane, J. M. C., Saltzman, E. S., Wiedensohler, A., and



- 666 Heard, D. E.: The chemistry of OH and HO₂ radicals in the boundary layer over the tropical Atlantic
667 Ocean, Atmos. Chem. Phys., 10, 1555-1576, 10.5194/acp-10-1555-2010, 2010.
- 668 Whalley, L. K., Blitz, M. A., Desservettaz, M., Seakins, P. W., and Heard, D. E.: Reporting the
669 sensitivity of laser-induced fluorescence instruments used for HO₂ detection to an interference from
670 RO₂ radicals and introducing a novel approach that enables HO₂ and certain RO₂ types to be
671 selectively measured, Atmos. Meas. Tech., 6, 3425-3440, 10.5194/amt-6-3425-2013, 2013.
- 672 Zhou, S. M., Shiraiwa, M., McWhinney, R. D., Poschl, U., and Abbatt, J. P. D.: Kinetic limitations in
673 gas-particle reactions arising from slow diffusion in secondary organic aerosol, Faraday Discuss., 165,
674 391-406, 10.1039/c3fd00030c, 2013.
- 675 Zobrist, B., Soonsin, V., Luo, B. P., Krieger, U. K., Marcolli, C., Peter, T., and Koop, T.: Ultra-slow
676 water diffusion in aqueous sucrose glasses, Phys. Chem. Chem. Phys., 13, 3514-3526,
677 10.1039/c0cp01273d, 2011.
- 678